THE JOURNAL OF PHYSICAL CHEMISTRY A

Article

Cite This: J. Phys. Chem. A 2017, 121, 8453-8464

pubs.acs.org/JPCA

Speciated Monitoring of Gas-Phase Organic Peroxy Radicals by Chemical Ionization Mass Spectrometry: Cross-Reactions between CH_3O_2, $CH_3(CO)O_2$, $(CH_3)_3CO_2$, and c-$C_6H_{11}O_2$

Published as part of The Journal of Physical Chemistry virtual special issue "Veronica Vaida Festschrift".

Barbara Nozière*,† and David R. Hanson‡

†CNRS/IRCELYON, Villeurbanne, France

‡Augsburg College, Minneapolis, United States

Supporting Information

ABSTRACT: Organic peroxy radicals ("RO_2", with R organic) are key intermediates in most oxygen-rich systems, where organic compounds are oxidized (natural environment, flames, combustion engines, living organisms, etc). But, until recently, techniques able to monitor simultaneously and distinguish between RO_2 species ("speciated" detection) have been scarce, which has limited the understanding of complex systems containing these radicals. Mass spectrometry using proton transfer ionization has been shown previously to detect individual gas-phase RO_2 separately. In this work, we illustrate its ability to speciate and monitor several RO_2 simultaneously by investigating reactions involving CH_3O_2, $CH_3C(O)O_2$, c-$C_6H_{11}O_2$, and $(CH_3)_3CO_2$. The detection sensitivity of each of these radicals was estimated by titration with NO to between 50 and 1000 Hz/ppb, with a factor from 3 to 5 of uncertainties, mostly due to the uncertainties in knowing the amounts of added NO. With this, the RO_2 concentration in the reactor was estimated between 1×10^{10} and 1×10^{12} molecules cm^{-3}. When adding a second radical species to the reactor, the kinetics of the cross-reaction could be studied directly from the decay of the first radical. The time-evolution of two and sometimes three different RO_2 was followed simultaneously, as the CH_3O_2 produced in further reaction steps was also detected in some systems. The rate coefficients obtained are (in molecule^{-1} cm^3 s^{-1}): $k_{CH3O2+CH3C(O)O2} = 1.2 \times 10^{-11}$, $k_{CH3O2+t\text{-}butylO2} = 3.0 \times 10^{-15}$, $k_{c\text{-}hexylO2+CH3O2} = 1.2 \times 10^{-13}$, $k_{t\text{-}butylO2+CH3C(O)O2} = 3.7 \times 10^{-14}$, and $k_{c\text{-}hexylO2+t\text{-}butylO2} = 1.5 \times 10^{-15}$. In spite of their good comparison with the literature and good reproducibility, large uncertainties (×5/5) are recommended on these results because of those in the detection sensitivities. This work is a first illustration of the potential applications of this technique for the investigation of organic radicals in laboratory and in more complex systems.

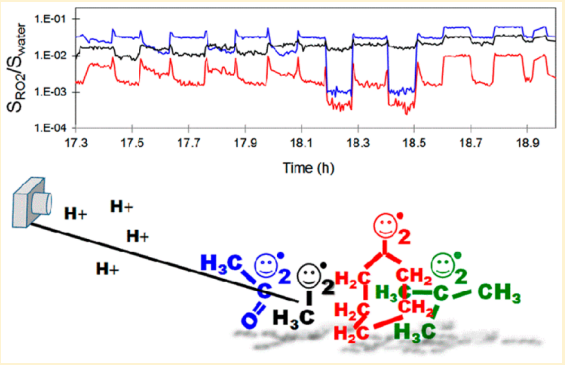

INTRODUCTION

Organic peroxy radicals ("RO_2", with R organic) are key species produced during the oxygen-based (or "aerobic") combustion of organic compounds and thus ubiquitous in the natural environment (atmosphere, surface waters, natural fires, etc), technological processes (combustion engines, power production) and even in living organisms. As their organic structure strongly affects their reactivity, information on their individual reactions is key to the understanding of such oxidation systems and the prediction of their outcome (ozone formation in the atmosphere, preignition in engines, etc). Unfortunately, classical monitoring techniques for RO_2, such as UV absorption, electron spin resonance (ESR),[1,2] and electron paramagnetic resonance (EPR; with or without spin trapping), cannot differentiate between different radicals. These techniques thus require even the simplest radical system to be analyzed with complex kinetic models, involving a number of assumptions, resulting, at best, in large uncertainties in the results and, at worse, in overlooking important reaction channels such as those identified over the past decade.[3−7] As emphasized in reviews of the topic,[3] such technical limits have been the main obstacle to the investigation of RO_2 reaction kinetics even in laboratory. Techniques monitoring simultaneously and distinguishing between different RO_2 ("speciated" detection) in more complex systems have also been lacking, which has limited the progress of all the fields of research mentioned above. In atmospheric chemistry, indirect techniques have been developed to monitor the RO_2 in the atmosphere, which consist in converting all the RO_2 into one single species, which is monitored: reacting the RO_2 with NO

Received: July 2, 2017
Revised: September 27, 2017
Published: October 16, 2017

DOI: 10.1021/acs.jpca.7b06456
J. Phys. Chem. A 2017, 121, 8453−8464

and monitoring either the NO_2 produced by luminescence ("PERCA")[8] or the HO_2 radical produced by laser-induced fluorescence (ROxLIF[9] and FAGE[10]); or reacting the RO_2 with labeled $^{34}SO_2$ to produce $H_2{}^{34}SO_4$, which is measured by mass spectrometry (ROxMAx[11] or PerCIMS[12]). While these techniques are valuable, and the only tools providing information on atmospheric RO_2 so far, they lose all information on the individual radicals and provide an overall RO_2 signal (or "ΣRO_2"). This information is not detailed enough to describe accurately the atmospheric radical cycles, as shown by the discrepancies between measured and modeled atmospheric radical levels.[13,14] Even the semispeciation between saturated and unsaturated (alkenes and aromatic) RO_2s proposed with FAGE[10] does not account for the orders of magnitude of difference in reactivity within each class of radicals (for instance, between $(CH_3)_3CO_2$ and $CH_3C(O)O_2$ among the saturated ones). Very recent works propose the specific detection of CH_3O_2 by conversion into CH_3O, which is then measured by LIF,[15] but not of other RO_2s.

Mass spectrometry (MS), when combined with a mild ionization technique avoiding fragmentation, is intrinsically speciated, because the ions produced are directly linked to the molecules or radicals analyzed through their mass (or mass/charge ratio, m/z). Numerous chemical ionization techniques for RO_2 have thus been explored since the 1980s, but few were found suitable to all types of RO_2s or systems: electron transfer with SF_6^-, O_2^-,[16,17] or excited rare gas[18] are only applicable to low-pressure systems; reactions with I^- or O_3^- only work with acylperoxyl radicals (R−C(O)−O_2);[17] reaction with O_2^+ leads to some fragmentations of the radicals (75% for CH_3O_2).[19] More recently, chemical ionization with NO_3^- was shown to detect highly oxidized C10−C12 RO_2 radicals ("HOMs") and used to monitor them in smog chamber,[20−24] and also possibly in the atmosphere,[20] although this was not confirmed. But this technique does not detect smaller, more volatile RO_2s that control the atmospheric radical cycles (CH_3O_2, $CH_3C(O)O_2$, etc). By contrast, proton transfer with H_3O^+ and water clusters, $H_3O^+(H_2O)_n$, which is based on the following ionization reaction:

$$RO_2 + H_3O^+(H_2O)_n \rightarrow RO_2H^+(H_2O)_m + (n - m + 1)H_2O \quad (1)$$

seems to be efficient with all the RO_2 explored so far (CH_3O_2, $C_2H_5O_2$, $CH_3C(O)O_2$, iso-$C_3H_7O_2$, c-$C_6H_{11}O_2$)[25−30] and does not result in fragmentation. It is thus promising for application to complex systems. While previous work has demonstrated the detection of individual gas-phase RO_2 by this technique,[25−30] the present work explores its ability to monitor simultaneously different radicals and illustrates the advantages to be gained in their investigation. The radical production system and flow reactor conditions, which were similar to those in ref 30, probably hold an advantage over the turbulent flow reactor technique of Elrod and co-workers,[25−29] by allowing for longer reaction times and possibly larger radical production with the UV lights.

In this work, CH_3O_2, $CH_3C(O)O_2$, $(CH_3)_3CO_2$, and c-$C_6H_{11}O_2$ were first produced individually in a flow reactor, and their spectra were characterized. CH_3O_2 and $CH_3C(O)O_2$ were chosen for their relevance in the atmosphere, and $(CH_3)_3CO_2$ and c-$C_6H_{11}O_2$ were selected to explore more complex mechanisms and very slow kinetics. Various amounts of NO were then added to the reactor to titrate the radicals and estimate their detection sensitivities. Finally, a second radical was added periodically to each radical system, and the kinetics of their cross-reactions was investigated, for the first time, from the decays of the individual radicals. In particular, the rate coefficients for the cross-reactions between CH_3O_2 and $CH_3C(O)O_2$, and between CH_3O_2 and $(CH_3)_3CO_2$, which are known in the literature, were remeasured to validate the method used in this work.

MATERIALS AND METHODS

Flow System and Radical Generation. The radicals were generated and reacted in a cylindrical glass reactor (inner diameter: 5 cm, length: 120 cm, Figure 1) disposed vertically, in

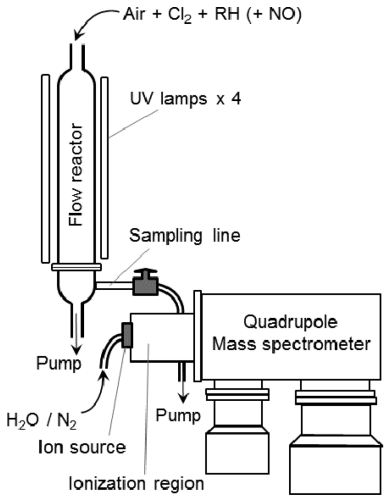

Figure 1. Schematic of the experimental setup.

an air flow (2−4 sLm, standard temperature = 273 K and pressure = 1 atm) near atmospheric pressure (0.6−0.9 atm). Typical residence times in the reactor were thus between 30 s and 1 min. Reynold's numbers for the flows were between 100 and 150, thus well in the laminar regime, with a mixing length of ∼25 cm. The organic precursors, CH_4, CH_3CHO, $CH(CH_3)_3$, or c-C_6H_{12}, each from 1×10^{13} to 1×10^{16} molecule cm^{-3}, and Cl_2 (2×10^{15} molecule cm^{-3}) were mixed into the air flow and introduced in the reactor through the top inlet. As this inlet was situated 10 cm above the reactor itself, this ensured that all the gases were mixed within the top 15 cm (∼10%) of the reactor. The radicals were produced by irradiating the reactor over 280−400 nm with four fluorescent lights (Philips TL12, 40 W) placed symmetrically at 2−3 cm around it. This led to the formation of Cl atoms:

$$Cl_2 + h\nu \rightarrow 2Cl \quad (2)$$

which, then, reacted with the organic precursors to produce each RO_2 radical. For CH_3O_2:

$$Cl + CH_4 \rightarrow CH_3 + HCl \quad (3)$$

$$CH_3 + O_2 + M \rightarrow CH_3O_2 + M \quad (4)$$

For the $CH_3C(O)O_2$ radical:

$$Cl + CH_3CHO \rightarrow CH_3C(O) \quad (5)$$

$$CH_3C(O) + O_2 + M \rightarrow CH_3C(O)O_2 + M \quad (6)$$

DOI: 10.1021/acs.jpca.7b06456
J. Phys. Chem. A 2017, 121, 8453−8464

Irradiation tests performed on CH_3CHO and in the absence of Cl_2 in the reactor showed that this compound was not photolyzed by the UV lights.

For the $(H_3C)_3CO_2$ radical:

$$Cl + (H_3C)_3CH \rightarrow (H_3C)_3C + HCl \quad (7)$$

$$(H_3C)_3C + O_2 + M \rightarrow (H_3C)_3CO_2 + M \quad (8)$$

And for the c-$C_6H_{11}O_2$ radical:

$$Cl + c\text{-}C_6H_{12} \rightarrow c\text{-}C_6H_{11} + HCl \quad (9)$$

$$c\text{-}C_6H_{11} + O_2 + M \rightarrow c\text{-}C_6H_{11}O_2 + M \quad (10)$$

Different configurations were used in the experiments: either the reactor was irradiated over its entire length or only on the bottom 50 cm (the top part being covered with aluminum foil). Although the second configuration made the production and observation of the radicals slightly easier to control, both gave similar spectra and kinetic results and were thus not differentiated in the results presented here.

Sampling and Detection. A schematic of the experimental setup is presented in Figure 1. The gas mixtures and RO_2 radicals present in the reactor were sampled for analysis into a quadrupole mass spectrometer built for this project and similar to the one described in refs 30 and 31. But, while in the previous setups with this type of instrument, the output of the reactor was directly integrated to the ionization region of the mass spectrometer,[25−30] in this work the sampling was performed through a line (~10 cm, diameter 1/4 in.) connecting the bottom outlet of the reactor to the ionization region of the mass spectrometer and equipped with a valve to keep the pressure in the ionization region independent from that in the flow reactor. This ionization region was a cylinder (Delrin, 5 cm of diameter × 5 cm in length) operated at a total pressure from 10 to 15 mbar. Flowing small concentrations of water (<10%) in a flow of N_2 (20−40 sccm) through a source maintained at high voltage (typically +800 V) produced a distribution of reagent ions, $H_3O^+(H_2O)_n$ with n = 1 to 5. The typical ion drift time in the ionization region was ~0.3 ms.

Depending on the conditions in the ionization region (temperature, relative humidity), the most abundant ions were for n = 2 (m/z = 55) or n = 3 (m/z = 73). These ions were accelerated toward the entrance of the mass spectrometer chamber by the voltage difference between the source (+800 V) and the spectrometer entrance (+20 V). The sampling flow from the reactor (typically 30 sccm) was introduced into the ionization region radially, at approximately two-thirds of its length, so that the sampling flow and the beam of reagent ions mixed efficiently. The signal intensities for various compounds in the spectra varied roughly between 100 and 1 × 10^5 Hz, with background signals between 1 and 100 Hz. Mass spectra were recorded with 0.1 amu increments.

As the humidity in the ionization region affected the detection sensitivity for the RO_2 (see ref 30 and next section) the ratio of the signal intensities for the two main water clusters, S_{73}/S_{55}, was used as a proxy for these conditions and as a variable when describing the detection sensitivities. Note that all the analyses presented in this work (calibrations, kinetic studies), are based on the ratios of the radical signals to the total reagent ion signal (or "water signal") instead of absolute signals (in Hz) to account for potential changes in the detection sensitivities during the experiments. The detection sensitivities reported in this work (in Hz/ppb) were thus calculated for a total reagent ion signal of 1 × 10^6 Hz. However, the water proton signals (especially S_{55} and S_{73}) often exceeded the linear range (for count rate) of the electron multiplier; thus, the sensitivities reported in this work cannot be compared to theoretical sensitivities, nor can they be converted into equivalent ion−molecule rate coefficients.

Determination of the Radical Concentrations and Rate Coefficients. The method used in this work to determine the RO_2 concentrations and detection sensitivities was similar to the one used in our previous study,[30] and it is illustrated in Figure 2: various concentrations of NO (typically

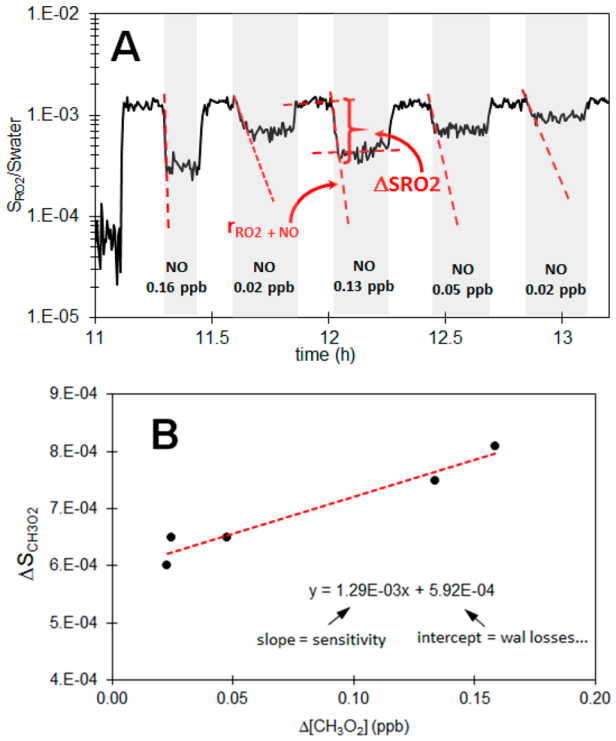

Figure 2. Determination of the detection sensitivity by titration with NO for CH_3O_2 (m/z = 84, experiment of Sept 30, 2015). (A) Evolution of S_{RO2} with time upon addition of different levels of [NO] and determination of r_{RO2+NO} and ΔS_{RO2}. (B) Determination of the detection sensitivity from the slope of ΔS_{RO2} vs $\Delta[RO_2]$.

0.05 to 2 ppb) were added to the reactor, alternating cycles with ON on and NO off. The decrease in RO_2 concentration, $\Delta[RO_2]$, upon adding NO, observed by the decrease in signal ΔS_{RO2}, was then assumed to result from the consumption of each RO_2 by 1 equiv of NO. The detection sensitivity, Sens(RO_2), was thus given by the ratio

$$\text{Sens}(RO_2) = \frac{\Delta S_{RO2}}{\Delta[RO2]} = \frac{\Delta S_{RO2}}{[NO]} \quad (11)$$

However, in our work, the added (or initial) [NO] could not be determined precisely from the instrument settings, because it was introduced in very small flows and because of significant losses of NO (and conversion to HONO) to the walls of the system. Instead, added [NO] was determined from the initial decay rate of RO_2, r_{RO2+NO} (s^{-1}; Figure 2A), divided by the corresponding rate coefficient, k_{RO2+NO} (molecule cm^3 s^{-1}), taken from the literature:

DOI: 10.1021/acs.jpca.7b06456
J. Phys. Chem. A 2017, 121, 8453−8464

$$[NO] = \frac{r_{RO2+NO}}{k_{RO2+NO}} \quad (12)$$

assuming that NO was well-mixed at the level of the reactor where the measurements were made. The accuracy in this method and in the resulting radical detection sensitivities depended on the accuracy in measuring the decay rate r_{RO2+NO}, thus in correcting for or ruling out potential contributions of the instrument dynamic response, wall losses, and mixing effects. In addition, both the accuracy in measuring the decay rate and the equivalence between ΔS_{RO2} and added [NO] implied that both the decay rate and ΔS_{RO2} resulted only from the reaction between RO_2 and NO and were not impacted by other reactions, such as the self-reactions of the RO_2, and their reactions with HO_2 or other RO_2 in the system. The potential contributions of instrument response, wall losses, and mixing effects to the measured r_{RO2+NO} were eliminated by adding different levels of NO in the system and confirming that r_{RO2+NO} varied proportionally with [NO]. In particular, this was expected to eliminate potential biases due to mixing effects, as NO was added in very small flows in the reactor, and the flow and mixing patterns in the reactor were thus not expected to depend on [NO]. The component of ΔS_{RO2} not varying with [NO] was thus assumed to be free from mixing effects, and the sensitivity, Sens(RO_2), was determined from the slopes of ΔS_{RO2} versus [NO] (Figure 2B), instead of the ratio in eq 11. The potential contributions of the self-reactions and reactions with HO_2 or other RO_2 to the measured r_{RO2+NO} and ΔS_{RO2} will be discussed in the Results section.

The rate coefficients for the cross reactions were determined with a similar method: producing one radical, R_1O_2, continuously in the reactor and producing the second one, R_2O_2, periodically by switching the flow of the corresponding precursor on and off. Monitoring both radicals simultaneously allowed determination of the rate coefficients for their cross-reactions, k_{cross}, directly from the initial decay rate of R_1O_2, $r_{R1O2+R2O2}$ (s^{-1}):

$$k_{cross} = \frac{r_{R1O2+R2O2}}{[R_2O_2]} \quad (13)$$

As in the titration with NO, this method requires the equivalence between $[R_2O_2]$ and $\Delta[R_1O_2]$, thus that each R_1O_2 is consumed by one equiv of R_2O_2, with no contribution of other reactions. $\Delta[R_1O_2]$ was, in turn, obtained from the corresponding signals, ΔS_{R1O2}, and the detection sensitivity obtained from the titration experiments, Sens(R_1O_2). Potential contributions of instrument response, wall losses, or mixing to the measured $r_{R1O2+R2O2}$ decays were also eliminated by varying $[R_2O_2]$ in the reactor. As with NO, flow patterns and mixing times in the reactor were not expected to vary with $[R_2O_2]$, as the organic precursors were introduced in small flows compared to the total flow. For all the radicals and over the range of concentrations studied, $r_{R1O2+R2O2}$ varied proportionally with $[R_2O_2]$; thus, k_{cross} was determined from the component of $r_{R1O2+R2O2}$ varying with $\Delta[R_1O_2]$, rather than from the ratio in eq 13. To validate this method two rate coefficients already known in the literature, namely, $k_{CH3O2+CH3C(O)O2}$ and $k_{CH3O2+t\text{-}butylO2}$, were remeasured in this work.

Chemicals. High-pressure gas mixtures of acetaldehyde and cyclohexane, each ~1% in N_2, were prepared by injecting known amounts of the pure liquids (typically, ~6 mL of acetaldehyde, >99.5%, Fluka, and 10 mL of cyclohexane >99%, Merck) in evacuated 6 L cylinders, measuring the resulting pressure change (typically, 300−500 mbar) and pressurizing the cylinders with N_2 to a total pressure between 50 and 100 bar.

All the other gas mixtures were purchased from manufacturers: N_2 quality 4.5, synthetic air 80/20, Cl_2, 1% in N_2, CH_4, 1% in N_2, isobutane, 1% in N_2, all Linde. NO, 1% in N_2, Air Liquide.

RESULTS AND DISCUSSION

Different series of experiments were performed in this work to characterize different aspects of the RO_2 reactivity, which are presented in sections (a) through (d) below. The complete list of experiments is given in Table S1 of the Supporting Information.

a. Radical Identification and Monitoring of All RO_2s in the System. The first step of this study was to make sure that the radicals produced in the reactor had the expected mass spectra (main peaks) and to determine potential interferences from other compounds on their masses. The ionization reaction 1 implies that a peroxy radical of molecular weight M produces ions of mass M+1, M+19, M+37, etc. Peaks corresponding to these masses were thus sought for in the mass spectra obtained when irradiating the reaction mixtures. However, the radicals reacted rapidly in the reactor, producing many stable products, following the generic reactions:[3,32]

$$RO_2 + RO_2 \rightarrow 2RO \quad (16)$$

$$\rightarrow \underline{ROH} + \underline{R'CHO} \quad (17)$$

$$\rightarrow \underline{ROOR} + O_2 \quad (18)$$

$$RO + O_2 \rightarrow \underline{R'CHO} + HO_2 \quad (19)$$

$$RO_2 + HO_2 \rightarrow \underline{ROOH} + O_2 \quad (20)$$

As proton transfer is sensitive to most oxygenated molecules, all the products underlined above were detected and resulted in much more intense signals than the radicals in the spectra. Thus, to isolate the RO_2 signals, NO was introduced periodically into the reactor, to remove the RO_2 rapidly, according to the reaction:

$$RO_2 + NO \rightarrow RO + NO_2 \quad (21)$$

The RO_2 spectra were thus obtained by subtracting the spectra of the reaction mixtures obtained in the absence and in the presence of NO. The results are presented in Figure 3. CH_3O_2 displayed almost exclusively an ion peak at m/z = 84 (n = 2 in eq 1, Figure 3A), although occasionally, under very dry conditions, the peak at m/z = 66 (n = 1) was observed. $CH_3C(O)O_2$ was mostly observed at m/z = 94 (n = 1 in eq 1, Figure 3B) but occasionally also at m/z = 112 (n = 2). $(CH_3)_3CO_2$ displayed two strong peaks at m/z = 108 (n = 1) and m/z = 126 (n = 2; Figure 3C), the relative intensity of which depended on the conditions in the reactor and ionization region; c-$C_6H_{11}O_2$ was the easiest radical to observe and displayed usually the most intense peak at m/z = 134 (n = 1 in eq 1, Figure 3D) but also significant ones at 152 (n = 2) and 170 (n = 3). In all cases, the peaks at n = 0 (m/z = 48 for CH_3O_2, m/z = 76 for $CH_3C(O)O_2$, m/z = 90 for $(CH_3)_3CO_2$, and m/z = 116 for c-$C_6H_{11}O_2$) were either not observed or strongly impacted by other species.

However, because NO was added at the top of the reactor, together with the organic precursors, it not only reacted with

DOI: 10.1021/acs.jpca.7b06456
J. Phys. Chem. A 2017, 121, 8453−8464

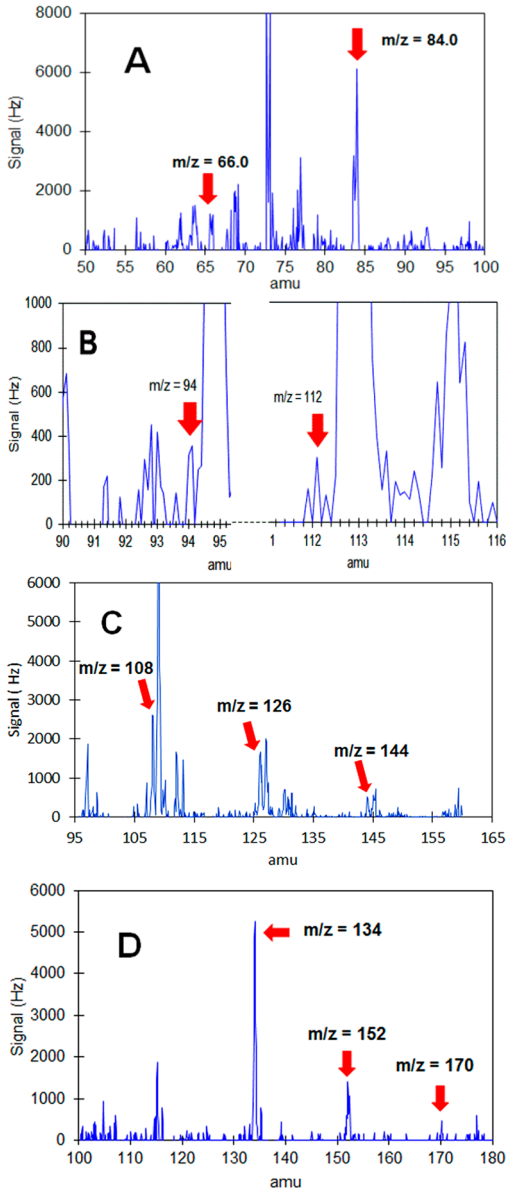

Figure 3. Mass spectra of the peroxy radicals: (A) CH_3O_2 (experiment of Sept 05, 2016); (B) $CH_3C(O)O_2$ (experiment of Dec 06, 2016); (C) $(CH_3)_3CO_2$ (experiment of May 10, 2017); (D) c-$C_6H_{11}O_2$ (experiment of June 14, 2016).

the RO_2 but also modified the product distribution. Thus, the major products formed in the absence of NO, such as ROOH, ROH, and ROOR, were also often visible in the difference spectra shown in Figure 3. Because ROOH is only 1 amu away from RO_2, variations of the corresponding signals S_{ROOH} and S_{RO2} were compared to check that S_{RO2} was not impacted by ROOH. This was especially important for $CH_3C(O)O_2$ (Figure 3B), because the two peaks were not always entirely resolved. Typical S_{ROOH} versus S_{RO2} plots are presented in Figure S2 and show that, while these signals followed similar trends (as might be expected), they varied distinctively from each other and thus corresponded to distinct species (different signals corresponding to the same species would have appeared perfectly aligned).

In addition to the RO_2 produced directly by the precursors, the technique allowed for the detection of all other peroxy radicals present in the reactor. CH_3O_2 was thus observed in all the mixtures where $CH_3C(O)O_2$ was present, which was expected, as it is produced rapidly by its self-reaction:[32]

$$2CH_3C(O)O_2 \rightarrow 2CH_3C(O)O + O_2 \quad (22)$$

$$2CH_3C(O)O + M \rightarrow CH_3 + CO_2 + M \quad (23)$$

$$CH_3 + O_2 + M \rightarrow CH_3O_2 + M \quad (24)$$

CH_3O_2 was also observed in the mixtures where $(CH_3)_3CO_2$ was present, as it is also produced by its self-reaction:

$$2(CH_3)_3CO_2 \rightarrow 2(CH_3)_3CO + O_2 \quad (25)$$

$$\rightarrow (CH_3)_3COOC(CH_3)_3 + O_2 \quad (26)$$

$$(CH_3)_3CO + M \rightarrow CH_3COCH_3 + CH_3 + M \quad (27)$$

followed by reaction 24 producing CH_3O_2.

Thus, in the investigation of the cross-reactions, where a second radical was added periodically to each radical system (see details in section d, below), up to three different RO_2 were observed simultaneously (Figure 4).

Occasionally, small amounts of other radicals due to contamination were observed in the reactor. For instance,

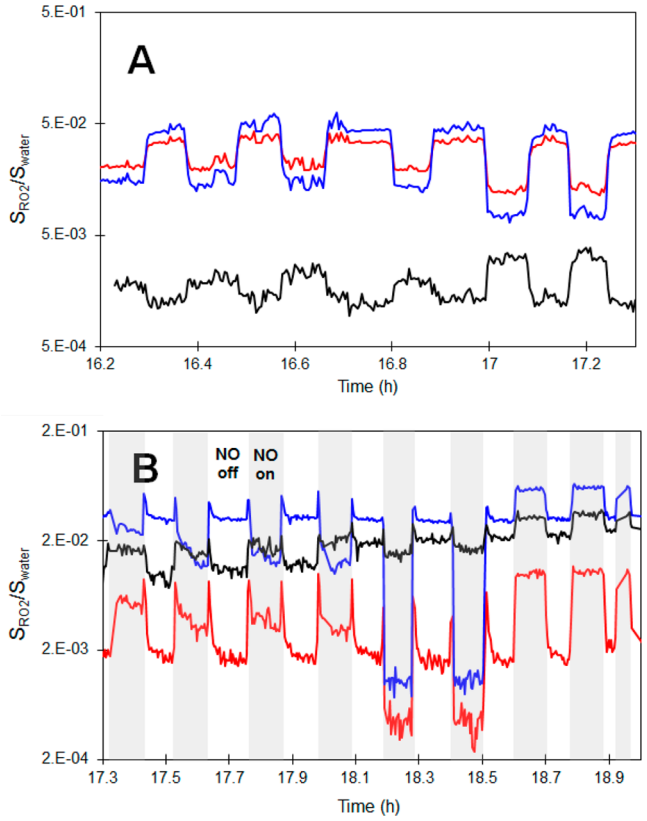

Figure 4. Simultaneous monitoring of three different RO_2 with the CIMS technique: (A) Real-time evolution of the signals for CH_3O_2 (black, m/z = 84), $CH_3C(O)O_2$ (red, m/z = 94), and $(CH_3)_3CO_2$ (blue, m/z = 108) upon periodic addition of CH_3CHO to a system in which isobutane is present continuously (experiment of June 7, 2017). Note that the apparent decay of $CH_3C(O)O_2$ upon addition of CH_3CHO is due to a change in the total signal; (B) Real-time evolution of the signals for CH_3O_2 (black, m/z = 84), $(CH_3)_3CO_2$ (blue, m/z = 108) and c-$C_6H_{11}O_2$ (red, m/z = 134) upon addition of various levels of NO in a system where both isobutane and c-hexane are present continuously (experiments of June 8, 2017).

DOI: 10.1021/acs.jpca.7b06456
J. Phys. Chem. A 2017, 121, 8453−8464

small amounts of c-$C_6H_{11}O_2$ were observed up to 2 d after performing experiments with cyclohexane. This had small impacts on the concentrations of the main radical studied, but the ability to detect unexpected radicals in the system confirmed the advantage of the chemical ionization mass spectrometry (CIMS) technique and its ability to investigate RO_2 chemistry in complex systems.

b. Time Evolution of the Radicals: Decays with HO_2 and "Intensification Effects" at Low [NO]. Observing the evolution of the signals for the individual RO_2s as a function of time (or "Single Ion Mode") with a resolution of a few seconds revealed several kinetic effects, which gave some indications on the reactions controlling the RO_2 steady-state concentrations in the reactor and decay rates. One of these effects was that, for all the radicals studied except $CH_3C(O)O_2$, after stopping NO or switching the lamps on, [RO_2] displayed a sharp increase followed by a fast decay, relaxing into a steady-state level after a few minutes (Figure 5A for c-$C_6H_{11}O_2$ and Figure S3 for CH_3O_2 and $(CH_3)_3O_2$). None of the stable reaction products monitored at the same time (ROOH, ROH, etc.; Figure 5A) displayed such decays, which ruled out flow or mixing effects, or changes in the detection performance as the explanation for these decays. The contrast between these fast decays and the steady profiles for the stable products (Figures 5A and S3) further confirmed that the signals had been correctly attributed between radicals and stable compounds. The sharp initial increase of [RO_2] was attributed to the nearly instantaneous production of the radicals by irradiation and reactions of Cl with the organic precursors, and the following fast decay to their self-reaction and buildup of other species, in particular, HO_2, in turn reacting with the RO_2. Thus, for radicals such as CH_3O_2 and c-$C_6H_{11}O_2$, producing HO_2 in their self-reaction (eq 19), the decays and steady-state concentration was expected to be controlled by their self-reaction or/and by their reaction with HO_2. For $(CH_3)_3CO_2$ and $CH_3C(O)O_2$ (eqs 22−24 and 25−27), which do not produce HO_2 in their self-reaction but CH_3O_2, the decays and steady-state concentrations were expected to result from the self-reactions (mostly for $CH_3C(O)O_2$), cross-reactions with CH_3O_2, and reactions with the HO_2 produced by CH_3O_2. With CH_3O_2, $(CH_3)_3CO_2$, and c-$C_6H_{11}O_2$, the formation of stable products, in particular, of ROOH was observed over the same time scale as these decays (Figures 5A and S3), confirming that the RO_2 + HO_2 reactions took place. With $CH_3C(O)O_2$ no decays were observed, suggesting that they were too fast to be monitored (>0.2 s^{-1}). The rate coefficient for the reaction of this radical with HO_2 being identical to that of other radicals,[33] this reaction could not account for such very fast decays. The decays and steady-state concentration of $CH_3C(O)O_2$ in the reactor were thus expected to be controlled by its self-reaction (which is the fastest known self-reaction of RO_2) and/or by its cross-reaction with CH_3O_2.

Another interesting kinetic effect was that, for all the radicals studied except $CH_3C(O)O_2$, adding very small amounts of NO to the reaction mixture resulted in larger RO_2 concentration than with [NO] = 0 ("intensification effect", Figure 5B for $(CH_3)_3CO_2$ and S4 for the other radicals). Only for larger amounts of NO the RO_2 started to be consumed. The intensification effects were attributed to NO consuming first (i.e., reacting faster with) the species acting as main sink for the RO_2s in the reactor, thus presumably HO_2. The net reduction of [RO_2] observed at larger [NO] was attributed to the consumption of all HO_2, leaving only RO_2 to react with NO.

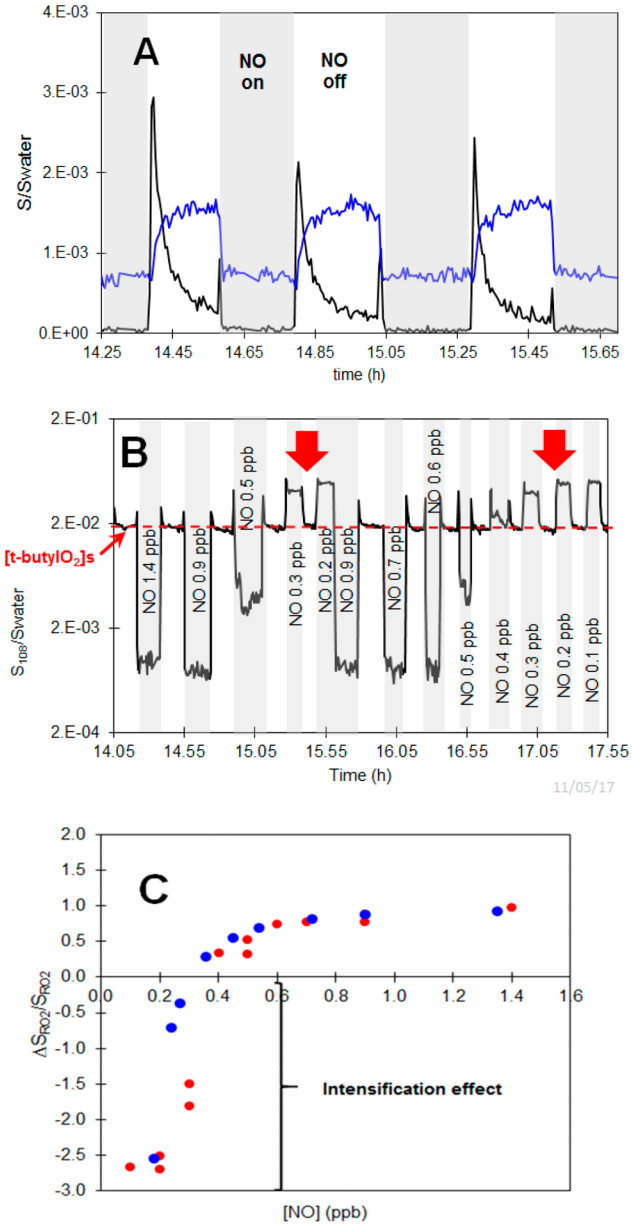

Figure 5. Real-time, steady-state, and relative variations of the RO_2 signal in the reactor upon addition of [NO]. (A) Real-time decay for c-$C_6H_{11}O_2$ (black line, m/z = 134) due to RO_2 + HO_2, compared with the profiles for c-$C_6H_{11}OOH$ (blue line, m/z = 135), experiment of June 14, 2016. (B) Variations of S_{RO2} with [NO] and intensification effect for $(CH_3)_3CO_2$ (m/z = 108, experiment of May 11, 2017). (C) Comparison of the observed $\Delta S_{RO2}/S_{RO2}$ (red symbols) with calculated ones (blue symbols for complete equation, white symbols without the self-reaction) for the experiment shown in (B).

The absence of intensification effect with $CH_3C(O)O_2$ at low [NO] was consistent with the fact that HO_2 was not a significant sink for this radical and that CH_3O_2, its expected main sink, did not react faster with NO than $CH_3C(O)O_2$ itself.

To verify these hypotheses and quantify the contribution of the different reactions to the radical concentrations in the reactor, [RO_2] was calculated and compared to the experiments. Details on these zero-dimensional (0D) calculations are given in Section S5, and the rate constants used are given in Table S6A. Briefly, they included a source term, F (molecule

DOI: 10.1021/acs.jpca.7b06456
J. Phys. Chem. A 2017, 121, 8453−8464

cm^{-3} s^{-1}), accounting for the production of the RO_2 by irradiation and reaction of Cl with the precursors, first-order losses to the walls and in the exit flow (mathematically indistinguishable), the RO_2 self-reactions and reactions with HO_2, CH_3O_2, and NO, and an additional source term specific to the presence of NO, F'_{NO} (molecule cm^{-3} s^{-1}), accounting for the potential recycling of HO_2 into HO, in turn producing rapidly RO_2. Because, at that point of the analysis, the absolute concentrations of RO_2 were not known, the comparisons with the experiments were based on the relative signal change $\Delta S_{RO2}/S_{RO2} = ([RO_2]_o - [RO_2]_s)/[RO_2]_o$, where $[RO_2]_o$ and $[RO_2]_s$ are the radical steady-state concentrations in the absence and in the presence of NO, respectively. Note that, here, "steady-state" defines concentrations that are constant in time, due to the equilibration of the different contributions listed above (thus including source and exit flows, in addition to chemical terms). The values for k_{wall}, F, and F'_{NO} were adjusted so that the calculated $\Delta S_{RO2}/S_{RO2}$ matched the observed ones (Figure 5C for $(CH_3)_3CO_2$ and Figure S7 for the other radicals), which provided values for these constants (given in Table S6B). The observed $\Delta S_{RO2}/S_{RO2}$ were well-accounted for with $F = 1 \times 10^8$ molecule cm^{-3} s^{-1} for CH_3O_2 and 1×10^9 for the other radicals, consistent with the much smaller reaction rate of Cl with CH_4 than with the other precursors. k_{wall} was found to be identical for all RO_2s, with a value of ∼0.01 s^{-1}. The corresponding residence time, 100 s, was of the order of the residence time resulting from the flow rate in the reactor (30 s^{-1} min), thus suggesting that the exit flow was a large component of k_{wall}. The calculations also showed that, for CH_3O_2, $(CH_3)_3CO_2$, and c-$C_6H_{11}O_2$, the self-reactions and reactions with HO_2 contributed relatively little (≤20%) to the steady-state concentrations and that, unlike what was expected, the suppression of HO_2 at low [NO] did not account for the observed intensification effects ($\Delta S_{RO2}/S_{RO2} < 0$ in Figures 5C and S7). To account for these effects it was necessary to introduce an additional source F'_{NO}, corresponding to the recycling of HO_2 into OH, in turn producing more RO_2. As a confirmation, the observed $\Delta S_{RO2}/S_{RO2}$ were best accounted for by scaling F'_{NO} with $[HO_2]$. For CH_3O_2 and c-$C_6H_{11}O_2$, $[HO_2]$ and F'_{NO} varied inversely with [NO], and with $(CH_3)_3CO_2$, even more strongly (see Section S5). These additional sources thus resulted in an increase of the RO_2 sources by a factor of 2−5 over a very small range of very low [NO]. The threshold [NO] at which these effects disappeared and $[RO_2]_s$ started to decrease compared to $[RO_2]_o$ were estimated for each radical: 0.04 ppb for CH_3O_2, 0.3 ppb for $(CH_3)_3CO_2$, and 0.1 ppb for c-$C_6H_{11}O_2$ (Table S6B).

For $CH_3C(O)O_2$, the calculations showed that the self-reaction and cross-reaction with CH_3O_2 were the main contributions to the steady-state concentration, resulting in a weak variability $\Delta S_{RO2}/S_{RO2}$ with [NO] (Figure S7B). As the concentration of HO_2 was significant in this system, some recycling of HO_2 into OH and intensification effects could not be excluded, but the calculations showed that they would occur over a range of [NO] too low to be explored experimentally (≤0.01 ppb, Figure S7).

Above the threshold [NO] at which the intensification effects disappeared, most HO_2 was consumed, and the recycling sources became negligible. Thus, these recycling effects had no impact on the radical concentrations over the range of [NO] used in the determination of their detection sensitivities (next section).

The calculations allowed to determine the correction factors to apply to the observed ΔS_{RO2} to ensure equivalence with added [NO] in the titration experiments. Details are given in Section S5, and the results are presented in Table S6C. For the range of [NO] used in the titration experiments (next section), these corrections were mostly significant for CH_3O_2 (×0.4) and $CH_3C(O)O_2$ (×0.15) and much less (×1) for $(CH_3)_3CO_2$ or c-$C_6H_{11}O_2$. For all the radicals, they resulted mostly from the wall losses and reactions with CH_3O_2 (for $CH_3C(O)O_2$).

In addition to the experiments where NO was added to systems containing one or two RO_2, an experiment was performed where NO was added periodically to a system containing three different RO_2s: CH_3O_2, $(CH_3)_3CO_2$, and c-$C_6H_{11}O_2$ (Figure 4B). The mixture was similar as in the study of the cross-reaction between $(CH_3)_3CO_2$ and c-$C_6H_{11}O_2$ (see section d), except that both isobutane and c-C_6H_{12} were introduced continuously in the reactor. The objective was to examine the evolution of each individual RO_2 upon addition of NO. Figure 4B clearly shows that, over a certain range, [NO] had opposite effects on the different RO_2s: small amounts of NO (∼0.3 ppb) resulted in intensification effects for all three radicals (last three cycles on the right-hand side), intermediate amounts (∼0.7 ppb, first four cycles) consumed $(CH_3)_3CO_2$ but increased the concentrations of CH_3O_2 and c-$C_6H_{11}O_2$. Finally, larger amounts of NO (∼1.4 ppb, cycles 5 and 6) consumed all three radicals. Although expected, such opposite effects of NO on RO_2s have, to our knowledge, not been observed directly before. This is mostly because indirect and conversion techniques monitor the sum of the RO_2 concentrations, in which opposite effects compensate each other. Such effects are yet likely to occur in complex mixtures such as in smog chambers or the atmosphere, which underlines the interest of the present technique for the monitoring of RO_2s.

c. RO_2 Detection Sensitivities. As described in the Materials and Methods section, the detection sensitivities for the RO_2s, Sens(RO_2), and RO_2 concentrations were determined by titrating the radicals with NO and measuring the decrease of $[RO_2]_s$ compared to $[RO_2]_o$. This required to use NO concentrations larger than the threshold reported above for the intensification effects: ∼0.1−0.5 ppb for CH_3O_2, 0.01−0.05 ppb for $CH_3C(O)O_2$, and 0.5−2 ppb both for $(CH_3)_3CO_2$ and c-$C_6H_5O_2$. In addition, the contributions to intensification effects and HO_2 reaction were kept minimal by reducing the RO_2 concentrations in the reactor, by limiting either the amount of Cl_2 in the reactor or irradiation (only one set of lamps on). As explained above, Sens(RO_2) was obtained from the observed change in signal, ΔS_{RO2}, and the corresponding change in steady-state concentration, $\Delta[RO_2]$, assuming equivalence between $\Delta[RO_2]$ and added [NO]. [NO] was, in turn, determined from the rate of decay of the radical, r_{RO2+NO} (eq 12). To eliminate potential contributions of wall losses and mixing effects, different [NO] were added to the reactor to confirm that both r_{RO2+NO} and ΔS_{RO2} varied proportionally with [NO] (Figures 2B and S8 for all the titration experiments performed) and Sens(RO_2) was obtained from the slopes of ΔS_{RO2} versus [NO] rather than eq 11. In addition, the ΔS_{RO2} measured for CH_3O_2 and $CH_3C(O)O_2$ were corrected by the factors calculated in the previous section to ensure equivalence between $\Delta[RO_2]$ and added [NO]. The resulting sensitivities, calculated for a total reagent ion signal, $S_o = 1 \times 10^6$ Hz, are presented in Figure 6 and Table S9. They varied between 50 Hz/ppb for CH_3O_2 under humid conditions

DOI: 10.1021/acs.jpca.7b06456
J. Phys. Chem. A 2017, 121, 8453−8464

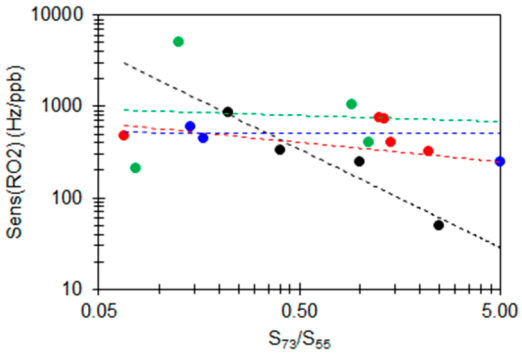

Figure 6. Detection sensitivities for the radicals as a function of the relative humidity in the ionization region, represented by the proxy, S_{73}/S_{55}. Black = CH_3O_2, m/z = 84; red = c-$C_6H_{11}O_2$, m/z = 134; blue = $(CH_3)_3CO_2$, m/z = 126; green = $CH_3C(O)O_2$, m/z = 94.

to ~5000 Hz/ppb for $CH_3C(O)O_2$ under dry conditions. These results can be compared with the radical theoretical sensitivity, calculated as in our previous work:[30]

$$TS = k_n t_d S_o \quad (29)$$

where k_n is the rate coefficient for the reaction between the radical and the reagent ion $H_3O^+(H_2O)_n$, t_d is the ion drift time, and S_o is the total ions signal, assumed equal to 1 MHz here. In our setup, for a drift length of 5 cm, a mobility of 130 cm/V and a voltage difference of 600 V, $t_d \approx 3 \times 10^{-4}$ s. In our previous work,[30] k_n was estimated to 2×10^{-9} molecules cm^{-3} s^{-1} for c-$C_6H_{11}O_2$ and decreasing with the radical molecular weight. This gives a maximum TS of 180 Hz/ppb for the RO_2s in the present work. Comparing with the sensitivities obtained experimentally thus suggested uncertainties of a factor 3 for c-$C_6H_{11}O_2$ and $(CH_3)_3CO_2$, and of approximately a factor 5 for CH_3O_2 and for most values obtained for $CH_3C(O)O_2$ (if ignoring the measurement at 5000 Hz/ppb). Of these uncertainties, up to approximately a factor 2, can possibly be attributed to the water proton signals exceeding the linear range of the electron multiplier, leaving the remaining uncertainties on the determination of [NO], thus the measurements of the decay rates. Both types of uncertainties can be improved in the future by reducing the total proton signal and by using a sensitive technique to monitor directly the small amounts of [NO] added to the reactor.

In spite of these large uncertainties, the results indicate a decrease of sensitivity with water vapor for all radicals (Figure 6), consistent with the one reported previously for CH_3O_2.[30]

Using these calibrations gave estimates for the RO_2 concentrations in the flow reactor between 1×10^{10} and 1×10^{12} molecules cm^{-3}. A typical background signal of 100 Hz in the instrument implied a detection limit between 1×10^8 and 1×10^9 molecules cm^{-3} for the radicals, similar to previous studies.[30]

d. Kinetics of Cross Reactions. As explained in "Material and Methods" the cross-reactions between different radicals were investigated by producing one radical, R_1O_2, continuously in the reactor and producing the second one, R_2O_2, periodically by switching the flow of the corresponding precursor on and off. For the first time, these cross-reactions could be observed directly by monitoring in real-time the decrease of R_1O_2 upon addition of R_2O_2 (Figure 7), and the rate coefficient k_{cross} could be determined from the corresponding decay rate $r_{R1O2+R2O2}$ (s^{-1}) instead of having to extract the individual information from complex signals, as with nonspeciated detection techniques. The concentration of added $[R_2O_2]$ was obtained from the signal change ΔS_{R1O2} and the detection sensitivity for R_1O_2 obtained in the previous section. As in the titration experiments, various $[R_2O_2]$ were added to the reactor to verify that $r_{R1O2+R2O2}$ varied proportionally (Figure S10), and k_{cross} was determined from the slope of r_{R1O2} versus $\Delta[R_1O_2]$ (Figure S10) rather than eq 13 to eliminate contributions of wall losses, mixing, and any other processes not varying with $[R_2O_2]$.

As in the reactions with NO, the radical concentrations had been lowered in the reactor to minimize the secondary reactions. In addition, to ensure equivalence between $\Delta[R_1O_2]$ and added $[R_2O_2]$ in the analyses, the correction factors to apply to the measured ΔS_{R1O2} were determined by performing similar calculations as for the titration experiments (Section S11): $\Delta S_{R1O2}/S_{R1O2}$ was calculated for various values of added $[R_2O_2]$ and compared with the experimental data. The results are presented in Figure S12. Very good agreements were obtained in all cases when using the constants determined in the previous calculations (k_{wall} and source term F). The correction factors x to apply to the observed ΔS_{R1O2}, $(\Delta S_{R1O2})_{obs}$, were determined as in the titration experiments, by calculating the ΔS_{R1O2} corresponding to equivalence, $(\Delta S_{R1O2})_{eq}$, by excluding the contributions of all reactions other than the wall losses (mostly, exit flow) and cross-reactions of interest. The correction factors obtained are given in Table S6C. For all the radicals and range of concentrations used in these experiments, they were similar to the correction factors used in the titration experiments (0.4 for CH_3O_2, 0.15 for $CH_3C(O)O_2$, and 1 for $(CH_3)_3CO_2$ and c-$C_5H_{11}O_2$). This was expected, as they resulted from the same reactions: wall losses (exit flow) and reactions with CH_3O_2. In each series of experiments, the average value for the rate coefficient was thus first determined by applying a linear regression to all the individual measurements of r_{R1O2} versus corrected $\Delta[R_1O_2]$. Then, compensating each measurement point for the slope and intercept of these regressions gave series of individual determinations for the same rate coefficients, presented in Table 1, which were used to estimate the statistical uncertainties in the results. The average values for the two coefficients that were already known, namely, $k_{CH3O2+CH3C(O)O2}$ and $k_{CH3O2+(CH3)3CO2}$, were in very good agreement with those recommended in the literature (see Table 1). In addition, the 17 individual measurements of $k_{CH3O2+CH3C(O)O2}$ and 11 individual measurements of $k_{CH3O2+(CH3)3CO2}$ were within 20 and 35% of the literature values. Although the other rate coefficients, $k_{c\text{-}hexylO2+CH3O2}$, $k_{t\text{-}butylO2+CH3C(O)O2}$, and $k_{c\text{-}hexylO2+t\text{-}butylO2}$, have not been reported before, to our knowledge, their average values were close to their expected values of $k_{cross} \approx \sqrt{(k_{self1} \times k_{self2})}$,[32] and the statistical dispersion on their 5 to 7 individual measurements were of 50% or less. These uncertainties are surprisingly small compared to the large uncertainties in the detection sensitivities (×5/5) and can be possibly attributed to some compensation between systematic errors, as shown by replacing eqs 11 and 12 in eq 13:

$$k_{cross} = \frac{\Delta S'_{R1O2}}{\Delta S_{R1O2}} \times \frac{r_{R1O2+R2O2}}{r_{R1O2+NO}} \times k_{R1O2+NO} \quad (30)$$

For instance, it was shown above that the correction factors on the ΔS_{RO2} were identical in the titration and cross-reaction experiments because they resulted from the same reactions. It is

DOI: 10.1021/acs.jpca.7b06456
J. Phys. Chem. A 2017, 121, 8453−8464

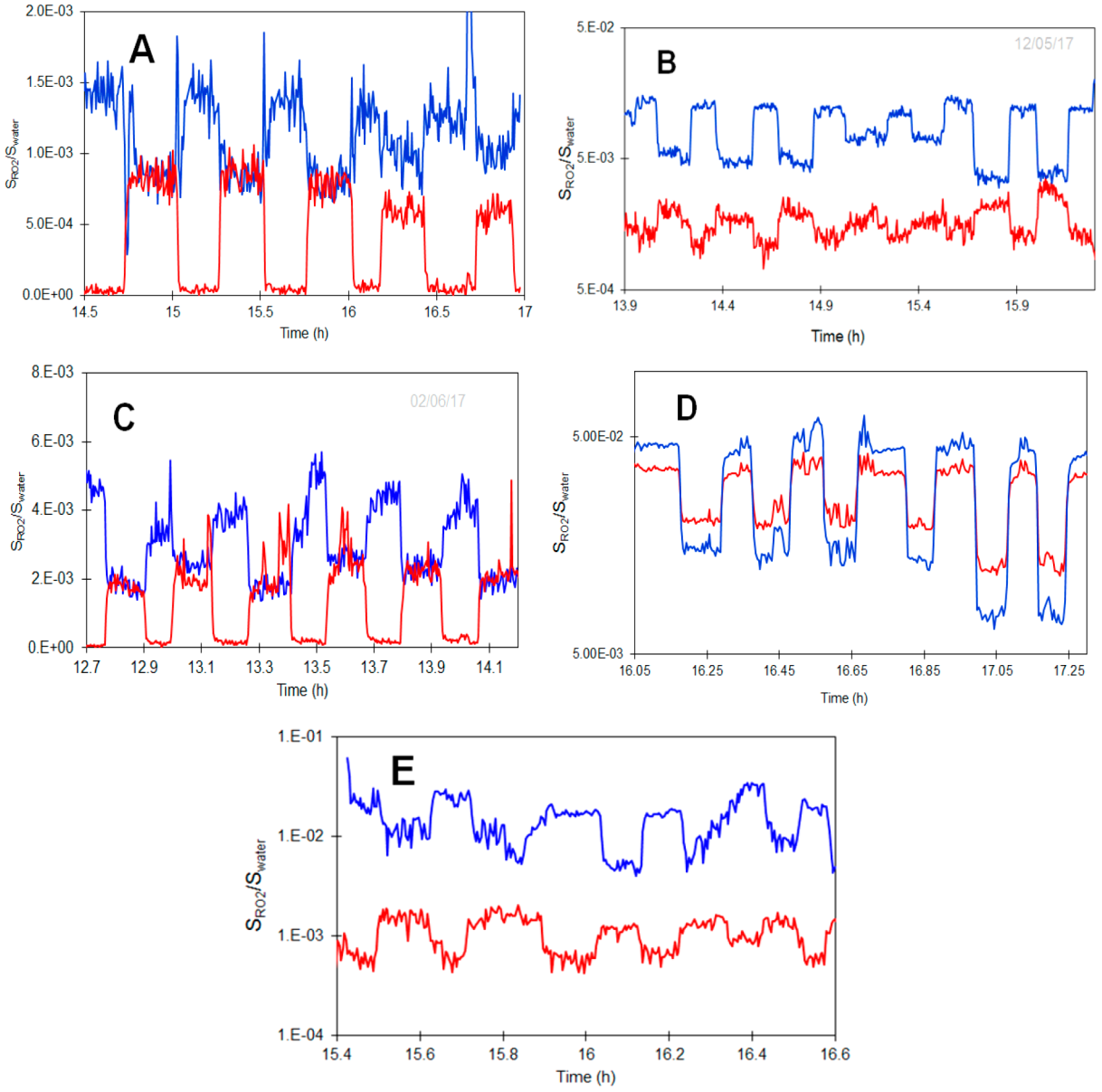

Figure 7. Real-time evolution of the signals for the different RO_2s in the cross-reactions experiments. Blue lines = R_1O_2 continuously present; red lines = R_2O_2, periodically added. (A) CH_3O_2 (red, m/z = 84) + $CH_3C(O)O_2$ (blue, m/z = 94), experiment of Oct 01, 2015; (B) CH_3O_2 (red, m/z = 84) + $(CH_3)_3CO_2$ (blue, m/z = 108), experiment of May 12, 2017; (C) CH_3O_2 (blue, m/z = 66) + c-$C_6H_{11}O_2$ (red, m/z = 134), experiment of June 02, 2017; (D) $CH_3C(O)O_2$ (red, m/z = 94) + $(CH_3)_3CO_2$ (blue, m/z = 108), experiment of June 07, 2017; (E) c-$C_6H_{11}O_2$ (red, m/z = 134) + $(CH_3)_3CO_2$ (blue, m/z = 108), experiment of June 08, 2017.

possible that, for instance, the decay rates are also systematically underestimated by not properly taking into account some mixing effects, which would result in similar errors in the titration and cross-reaction experiments, canceling each other out in eq 30. However, direct measurements of [NO] in the experiments and further model calculations, such as two-dimensional fluid dynamics reactor analysis, would be needed to identify the source of error in the current determinations of the RO_2 sensitivities and quantify those in the decay rate measurements. Until these uncertainties are identified and quantified, we recommend the same uncertainties in the reported rate coefficients as in the detection sensitivities, thus ×5/5.

CONCLUSIONS

This work illustrates the performance of the CIMS with proton transfer for the speciated detection of RO_2 in complex systems. Reported for the first time, two to three different RO_2 were monitored simultaneously, and their cross-reactions could be observed directly from the decay of one radical when a second one was produced. The rate coefficients for these cross-reactions were determined directly from the individual signals, instead of being extracted from overall signals with kinetic models, as with nonspeciated detection techniques. This opens the possibility for important improvements in the investigation of the kinetics of these species in the laboratory and ultimately in the understanding of the radical cycles in the atmosphere and other systems, by reducing the number of unknowns in the observations. The main uncertainties in this work were those

DOI: 10.1021/acs.jpca.7b06456
J. Phys. Chem. A 2017, 121, 8453−8464

Table 1. Rates Constants for the Cross-Reactions Measured in This Work

	R_1O_2 m/z	S_{73}/S_{55}	$Sens_{R1O2}$ (Hz/ppb)	k_{cross} (molecule^{-1} cm^3 s^{-1})	lit values
CH_3O_2 + $CH_3C(O)O_2$	$CH_3C(O)O_2$	0.6	750	1.42×10^{-11}	
				1.33×10^{-11}	
				1.14×10^{-11}	
				1.08×10^{-11}	
				1.01×10^{-11}	
Oct 01, 2015				ave = 1.20×10^{-11}	
June 06, 2017		0.07	750	8.70×10^{-12}	
				1.53×10^{-11}	
				1.18×10^{-11}	
				1.66×10^{-11}	
				1.32×10^{-11}	
				ave 1.31×10^{-11}	
	94				
June 07, 2017		0.13	5100	1.02×10^{-11}	
				1.55×10^{-11}	
				5.53×10^{-12}	
				1.34×10^{-11}	
				8.56×10^{-12}	
				1.10×10^{-11}	
				1.03×10^{-11}	
				ave = 1.06×10^{-11}	$(1.1 \pm 0.3) \times 10^{-11}$ ref 33
CH_3O_2 + $(CH_3)_3CO_2$	$(CH_3)_3CO_2$				
May 12, 2017	108	0.25	20	2.71×10^{-15}	
				3.28×10^{-15}	
				3.79×10^{-15}	
				2.74×10^{-15}	
				3.00×10^{-15}	
				3.60×10^{-15}	
				ave 3.2×10^{-15}	
May 16, 2017	126	15	2	2.45×10^{-15}	
				1.93×10^{-15}	
				2.45×10^{-15}	
				4.38×10^{-15}	
				3.14×10^{-15}	
				ave = 2.9×10^{-15}	$(3.0 \pm 0.3) \times 10^{-15}$ ref 32
CH_3O_2 + c-$C_6H_{11}O_2$	CH_3O_2 66	0.08	160	8.94×10^{-14}	
June 02, 2017				2.50×10^{-13}	
				8.96×10^{-14}	
				1.22×10^{-13}	
				6.17×10^{-14}	
				ave = 1.2×10^{-13}	
$CH_3C(O)O_2$ + $(CH_3)_3CO_2$	$(CH_3)_3CO_2$ 126	1	250	3.08×10^{-14}	
June 07, 2017				2.76×10^{-14}	
				3.74×10^{-14}	
				3.75×10^{-14}	
				5.09×10^{-14}	
				ave = 3.7×10^{-14}	
$(CH_3)_3CO_2$ + c-$C_6H_{11}O_2$	$(CH_3)_3CO_2$ 108	0.17	10	3.10×10^{-16}	
June 08, 2017				8.78×10^{-16}	
				1.80×10^{-15}	
				3.53×10^{-15}	
				1.05×10^{-15}	
				ave = 1.5×10^{-15}	

on the detection sensitivities estimated for the radicals (×5/5), which were mostly due to the difficulties in knowing the amounts of NO added to the reactor and in the determination of the radical decay rates. These uncertainties can be readily solved by experimental changes, such as measuring directly the small NO concentrations with a sensitive technique and by replacing time-dependent measurements by static methods, such as using a movable injector to introduce one radical precursor and measuring the changes in the steady-state concentrations. Until the source for these uncertainties has been identified, similarly large uncertainties (×5/5) are recommended on the reported rate coefficients, in spite of

DOI: 10.1021/acs.jpca.7b06456
J. Phys. Chem. A 2017, 121, 8453−8464

their apparent good comparison with the literature and good reproducibility.

One advantage of the technique used in this work was to monitor in real time individual RO_2 radicals and their nonsteady-state kinetic effects (fast increase and decays in RO_2 concentrations). Another advantage was to monitor simultaneously different RO_2s and observe directly their opposite behaviors (increase or decrease in steady-state $[RO_2]$) at low [NO]. Many such effects are likely to take place in complex systems, such as the atmosphere, but are currently undetected by the nonspeciated (conversion) techniques. The CIMS technique would thus be a valuable tool to study RO_2 in more complex mixtures than in flow reactors, such as smog chambers, where it would greatly improve the understanding of the radical mechanisms and validation of models.

■ ASSOCIATED CONTENT

Supporting Information

The Supporting Information is available free of charge on the ACS Publications website at DOI: 10.1021/acs.jpca.7b06456.

List of the experiments presented in this manuscript. Comparisons of the signals at the RO_2 masses, S_{RO2}, with those at the ROOH masses, S_{ROOH}. Fast decays of the individual RO_2 observed after stopping the NO flow in the reactor. Steady-state $[RO_2]$ increase and decrease upon addition of NO in the reactor. Calculation of $\Delta S_{RO2}/S_{RO2}$ as a function of NO in the reactor. List of the kinetic constants used in the calculations of $\Delta S_{RO2}/S_{RO2}$ as a function of [NO]. Comparison between observed and calculated $\Delta S_{RO2}/S_{RO2}$ as a function of [NO] added in the reactor. ΔS_{RO2} versus [NO] plots used for the calibration of the detection sensitivities. Results of the detection sensitivity calibrations. r_{R1O2} versus ΔS_{RO2} plots used for the determination of the rate coefficients for the cross-reactions. Calculations of $\Delta S_{R1O2}/S_{R1O2}$ as a function of $[R_2O_2]$ in the cross-reactions. Calculated $\Delta S_{R1O2}/S_{R1O2}$ as a function of added $[R_2O_2]$ in the cross reactions (PDF)

■ AUTHOR INFORMATION

Corresponding Author

*E-mail: barbara.noziere@ircelyon.univ-lyon1.fr.

ORCID

Barbara Nozière: 0000-0001-5841-1310

David R. Hanson: 0000-0001-5719-377X

Author Contributions

The manuscript was written through contributions of all authors. All authors have given approval to the final version of the manuscript. B.N. helped to build the CIMS instrument used in the experiments, performed the experiments and analyses, and wrote the manuscript. D.H. designed and built the CIMS instrument and helped with writing some experimental parts of the manuscript (e.g., CIMS detection and highlighting experimental detail) and contributed to the discussion of the analysis.

Notes

The authors declare no competing financial interest.

■ ACKNOWLEDGMENTS

This work was funded by the National Science Foundation, Grant No. NSF-ATM 0232057, which is gratefully acknowledged by the authors. B.N. also warmly thanks the many people whose valuable help have made this work possible: L. Zink (then at NCAR, Boulder, CO) for building the CIMS instrument, M. Grasmueck (Univ. of Miami, FL) for transporting it to Univ. of Miami, and W. Esteve (then at Univ. of Miami) for setting it up, and M. Dupanloup (CNRS, Ircelyon, France) is gratefully thanked for repairing the CIMS detection system. Special thanks are due to H. Wegmann (Wegmann Marin) for transporting the instrument to Stockholm Univ., Sweden, and CNRS, France, helping to set it up, and for his constant support throughout this long project. Conversations with J. Orlando and G. Tyndall, NCAR, Boulder, CO, are also gratefully acknowledged.

■ REFERENCES

(1) Mihelcic, D.; Musgen, P.; Ehhalt, D. H. An improved method of measuring tropospheric NO_2 and RO_2 by matrix-isolation and electron-spin-resonance. *J. Atmos. Chem.* **1985**, *3*, 341−361.

(2) Fuchs, H.; Brauers, T.; Haseler, R.; Holland, F.; Mihelcic, D.; Musgen, P.; Rohrer, F.; Wegener, R.; Hofzumahaus, A. Intercomparison of peroxy radical measurements obtained at atmospheric conditions by laser-induced fluorescence and electron spin resonance spectroscopy. *Atmos. Meas. Tech.* **2009**, *2*, 55−64.

(3) Orlando, J. J.; Tyndall, G. S. Laboratory studies of organic peroxy radical chemistry: an overview with emphasis on recent issues of atmospheric significance. *Chem. Soc. Rev.* **2012**, *41*, 6294−6317.

(4) Dillon, T. J.; Crowley, J. N. Direct detection of OH formation in the reactions of HO_2 with $CH_3C(O)O_2$ and other substituted peroxy radicals. *Atmos. Chem. Phys.* **2008**, *8*, 4877−4889.

(5) Peeters, J.; Nguyen, T. L.; Vereecken, L. HOx radical regeneration in the oxidation of isoprene. *Phys. Chem. Chem. Phys.* **2009**, *11*, 5935−5939.

(6) Jenkin, M. E.; Hurley, M. D.; Wallington, T. J. Investigation of the radical product channel of the $CH_3OCH_2O_2$ + HO_2 reaction in the gas phase. *J. Phys. Chem. A* **2010**, *114*, 408−416.

(7) Peeters, J.; Muller, J.-F. HOx radical regeneration in isoprene oxidation via peroxy radical isomerisations. II: experimental evidence and global impact. *Phys. Chem. Chem. Phys.* **2010**, *12*, 14227−14235.

(8) Cantrell, C. A.; Stedman, D. H.; Wendel, G. J. Measurement of atmospheric peroxy-radicals by chemical amplification. *Anal. Chem.* **1984**, *56*, 1496−1502.

(9) Fuchs, H.; Holland, F.; Hofzumahaus, A. Measurement of tropospheric RO_2 and HO_2 radicals by a laser-induced fluorescence instrument. *Rev. Sci. Instrum.* **2008**, *79*, 12.

(10) Whalley, L. K.; Blitz, M. A.; Desservettaz, M.; Seakins, P. W.; Heard, D. E. Reporting the sensitivity of laser-induced fluorescence instruments used for HO_2 detection to an interference from RO_2 radicals and introducing a novel approach that enables HO_2 and certain RO_2 types to be selectively measured. *Atmos. Meas. Tech.* **2013**, *6*, 3425−3440.

(11) Hanke, M.; Uecker, J.; Reiner, T.; Arnold, F. Atmospheric peroxy radicals: ROXMAS, a new mass-spectrometric methodology for speciated measurements of HO_2 and sigma RO_2 and first results. *Int. J. Mass Spectrom.* **2002**, *213*, 91−99.

(12) Reiner, T.; Hanke, M.; Arnold, F. Atmospheric peroxy radical measurements by ion molecule reaction mass spectrometry: A novel analytical method using amplifying chemical conversion to sulfuric acid. *J. Geophys. Res.* **1997**, *102*, 1311−1326.

(13) Lelieveld, J.; Butler, T. M.; Crowley, J. N.; Dillon, T. J.; Fischer, H.; Ganzeveld, L.; Harder, H.; Lawrence, M. G.; Martinez, M.; Taraborrelli, D.; et al. Atmospheric oxidation capacity sustained by a tropical forest. *Nature* **2008**, *452*, 737−740.

(14) Hofzumahaus, A.; Rohrer, F.; Lu, K. D.; Bohn, B.; Brauers, T.; Chang, C. C.; Fuchs, H.; Holland, F.; Kita, K.; Kondo, Y.; et al.

DOI: 10.1021/acs.jpca.7b06456
J. Phys. Chem. A 2017, 121, 8453−8464

Amplified trace gas removal in the troposphere. *Science* **2009**, *324*, 1702−1704.
(15) Onel, L.; Brennan, A.; Seakins, P. W.; Whalley, L.; Heard, D. E. A new method for atmospheric detection of the CH_3O_2 radical. *Atmos. Meas. Technol. Discuss.* **2017**, *2017*, 1−20.
(16) Eberhard, J.; Villalta, P. W.; Howard, C. J. Reaction of isopropyl peroxy radicals with NO over the temperature range 201−401 K. *J. Phys. Chem.* **1996**, *100*, 993−997.
(17) Villalta, P. W.; Howard, C. J. Direct kinetics study of the $CH_3C(O)O_2$ + NO reaction using chemical ionization mass spectrometry. *J. Phys. Chem.* **1996**, *100*, 13624−13628.
(18) Kondow, T. Ionization of clusters in collision with high-Rydberg rare gas atoms. *J. Phys. Chem.* **1987**, *91*, 1307−1316.
(19) Villalta, P. W.; Huey, L. G.; Howard, C. J. A temperature-dependent kinetics study of the CH_3O_2 + NO reaction using chemical ionization mass spectrometry. *J. Phys. Chem.* **1995**, *99*, 12829−12834.
(20) Jokinen, T.; Sipilä, M.; Richters, S.; Kerminen, V.-M.; Paasonen, P.; Stratmann, F.; Worsnop, D.; Kulmala, M.; Ehn, M.; Herrmann, H.; et al. Rapid autoxidation forms highly oxidized RO_2 radicals in the atmosphere. *Angew. Chem., Int. Ed.* **2014**, *53*, 14596−14600.
(21) Berndt, T.; Richters, S.; Kaethner, R.; Voigtländer, J.; Stratmann, F.; Sipilä, M.; Kulmala, M.; Herrmann, H. Gas-phase ozonolysis of cycloalkenes: formation of highly oxidized RO_2 radicals and their reactions with NO, NO_2, SO_2, and other RO_2 radicals. *J. Phys. Chem. A* **2015**, *119*, 10336−10348.
(22) Mentel, T. F.; Springer, M.; Ehn, M.; Kleist, E.; Pullinen, I.; Kurtén, T.; Rissanen, M.; Wahner, A.; Wildt, J. Formation of highly oxidized multifunctional compounds: autoxidation of peroxy radicals formed in the ozonolysis of alkenes − deduced from structure−product relationships. *Atmos. Chem. Phys.* **2015**, *15*, 6745−6765.
(23) Richters, S.; Herrmann, H.; Berndt, T. Highly oxidized RO_2 radicals and consecutive products from the ozonolysis of three sesquiterpenes. *Environ. Sci. Technol.* **2016**, *50*, 2354−2362.
(24) Richters, S.; Pfeifle, M.; Olzmann, M.; Berndt, T. Endo-cyclization of unsaturated RO_2 radicals from the gas-phase ozonolysis of cyclohexadienes. *Chem. Commun.* **2017**, *53*, 4132−4135.
(25) Scholtens, K. W.; Messer, B. M.; Cappa, C. D.; Elrod, M. J. Kinetics of the CH_3O_2+NO reaction: Temperature dependence of the overall rate constant and an improved upper limit for the CH_3ONO_2 branching channel. *J. Phys. Chem. A* **1999**, *103*, 4378−4384.
(26) Ranschaert, D. L.; Schneider, N. J.; Elrod, M. J. Kinetics of the $C_2H_5O_2$+NO_x reactions: Temperature dependence of the overall rate constant and the $C_2H_5ONO_2$ branching channel of $C_2H_5O_2$+NO. *J. Phys. Chem. A* **2000**, *104*, 5758−5765.
(27) Elrod, M. J.; Ranschaert, D. L.; Schneider, N. J. Direct kinetics study of the temperature dependence of the CH_2O branching channel for the CH_3O_2+HO_2 reaction. *Int. J. Chem. Kinet.* **2001**, *33*, 363−376.
(28) Chow, J. M.; Miller, A. M.; Elrod, M. J. Kinetics of the $C_3H_7O_2$+NO reaction: Temperature dependence of the overall rate constant and the i-$C_3H_7ONO_2$ branching channel. *J. Phys. Chem. A* **2003**, *107*, 3040−3047.
(29) Miller, A. M.; Yeung, L. Y.; Kiep, A. C.; Elrod, M. J. Overall rate constant measurements of the reactions of alkene-derived hydroxyalkylperoxy radicals with nitric oxide. *Phys. Chem. Chem. Phys.* **2004**, *6*, 3402−3407.
(30) Hanson, D.; Orlando, J.; Noziere, B.; Kosciuch, E. Proton transfer mass spectrometry studies of peroxy radicals. *Int. J. Mass Spectrom.* **2004**, *239*, 147−159.
(31) Hanson, D. R.; Greenberg, J.; Henry, B. E.; Kosciuch, E. Proton transfer reaction mass spectrometry at high drift tube pressure. *Int. J. Mass Spectrom.* **2003**, *223*, 507−518.
(32) Lightfoot, P. D.; Cox, R. A.; Crowley, J. N.; Destriau, M.; Hayman, G. D.; Jenkin, M. E.; Moortgat, G. K.; Zabel, F. Organic peroxy-radicals - Kinetics, spectroscopy and tropospheric chemistry. *Atmos. Environ., Part A* **1992**, *26*, 1805−1961.
(33) Atkinson, R.; Baulch, D. L.; Cox, R. A.; Crowley, J. N.; Hampson, R. F.; Hynes, R. G.; Jenkin, M. E.; Rossi, M. J.; Troe, J.; et al. Evaluated kinetic and photochemical data for atmospheric chemistry: Volume II - gas phase reactions of organic species. *Atmos. Chem. Phys.* **2006**, *6*, 3625−4055.

DOI: 10.1021/acs.jpca.7b06456
J. Phys. Chem. A 2017, 121, 8453−8464